

# Charge transfer of polyatomic molecules in ion-atom hybrid traps: Stereodynamics in the millikelvin regime

Alexandre Voute,<sup>1,2,\*</sup> Alexander Dörfler,<sup>3</sup> Laurent Wiesenfeld,<sup>2</sup>  
Olivier Dulieu,<sup>2</sup> Fabien Gatti,<sup>1</sup> Daniel Peláez,<sup>1</sup> and Stefan Willitsch<sup>3,†</sup>

<sup>1</sup>*Université Paris-Saclay, CNRS, Institut des Sciences Moléculaires d'Orsay, 91405, Orsay, France.*

<sup>2</sup>*Université Paris-Saclay, CNRS, Laboratoire Aimé-Cotton, 91405, Orsay, France.*

<sup>3</sup>*Department of Chemistry, University of Basel, Klingelbergstrasse 80, 4056 Basel, Switzerland*

(Dated: July 12, 2023)

Rate constants for the charge transfer reaction between  $\text{N}_2\text{H}^+$  and Rb in the mK regime are measured in an ion-atom hybrid trap and are found to be lower than the Langevin capture limit. Multireference *ab initio* computation of the potential energy surfaces involved in the reaction reveals that the low-temperature charge transfer is hindered by short-range features highly dependent on the collision angle and is promoted by a deformation of the molecular frame. The present study highlights the importance of polyatomic effects and of stereodynamics in cold molecular ion-neutral collisions.

**Introduction.** Over the past decade, the advent of cold ion-atom hybrid trapping experiments has opened up a range of new research avenues in both physics and chemistry [1]. These include the exploration of new cooling mechanisms [2–5], the study of unusual light-driven reactive processes [6, 7], the characterization of many-body dynamics [8], and the investigation of ion-atom interactions in the quantum regime [9–12]. Many ion-atom hybrid systems turned out to be chemically reactive which for the first time opened up possibilities to explore ion-neutral chemical processes in the mK to  $\mu\text{K}$  temperature regimes, in particular charge exchange [6, 7, 13–15]. Charge transfer can either occur radiatively, i.e., the collision system transits between different electronic states by the emission of a photon, or non-adiabatically around crossing points between two electronic states with a different asymptotic charge character [16, 17]. Both scenarios have previously been observed and characterized in different ion-atom hybrid systems, with non-adiabatic charge exchange usually being considerably more efficient than its radiative counterpart [17, 18]. Both non-reactive and reactive collisional processes in hybrid traps have often been successfully analyzed in the framework of Langevin or modified Langevin models only taking into account the long-range interactions between the ion and the neutral [1, 9, 14, 18, 19].

A recent development is the introduction of molecular ions into hybrid experiments. The exquisite degree of control over temperatures and quantum states of the trapped particles achievable in hybrid traps provide an ideal environment for studying subtle details of molecular phenomena and interactions [5, 14, 15, 20, 21]. The increased complexity of molecular systems inevitably entails richer dynamics compared to atoms. Previous studies on cold interactions of diatomic ions such as  $\text{N}_2^+$  and  $\text{O}_2^+$  with alkali atoms [14, 15] revealed an intricate interplay between long and short-range interactions governing the dynamics and kinetics of charge exchange in different electronic states of the collisions system. In some

states, charge transfer rates were found to be compatible with the Langevin model which only considers ion-induced dipole long-range interactions. In other states, higher-order electrostatic interactions and, in particular, the specific dynamics around state crossings had to be taken into account in order to rationalize the charge transfer dynamics.

In the present study, we introduced polyatomic molecular ions into an ion-atom hybrid experiment to explore the ramifications of molecular complexity in cold charge-transfer dynamics with the example of the prototypical triatomic species  $\text{N}_2\text{H}^+$ , a stable linear cation well known from astronomical observations [22], laboratory experiments [23–26] and theoretical works [27–29]. We studied the charge transfer of  $\text{N}_2\text{H}^+$  with Rb atoms in their  $(5s) \ ^2S_{1/2}$  ground and  $(5p) \ ^2P_{3/2}$  excited electronic states at collision energies in the mK regime. In both states, we found charge-transfer rates below the Langevin limit. The experimental results were interpreted with the help of multireference *ab-initio* calculations of the lowest potential energy surfaces (PESs) of the  $[\text{N}_2\text{H}-\text{Rb}]^+$  collision system. The calculations reveal that the charge transfer dynamics uncovered here is governed by distinct short-range molecular effects which cannot be captured by simple Langevin-type models and highlight the relevance of stereodynamics in cold collisions of this polyatomic system.

**Experiments.** The experimental setup has been described in detail previous publications [15, 30]. Briefly, it consisted of an ion-neutral hybrid trap comprising a linear-quadrupole radiofrequency (RF) ion trap embedded in a magneto-optical trap (MOT) for the cooling and trapping of Rb atoms. The ion trap was operated at a frequency of  $\Omega_{\text{RF}} = 2\pi \times 3.25 \text{ MHz}$  with an amplitude of  $V_{\text{RF}} = 400 \text{ V}$  and featured 12 individual electrode segments for the application of static and RF voltages. The experimental sequence started with the loading of  $\text{Ca}^+$  ions produced from an effusive beam of Ca atoms by non-resonant photoionization. The  $\text{Ca}^+$  ions formed

Coulomb crystals [31] in the RF trap upon Doppler laser cooling on the  $(4s) ^2S_{1/2} \leftrightarrow (4p) ^2P_{1/2} \leftrightarrow (3d) ^2D_{3/2}$  optical cycling transitions using two laser beams at 397 and 866 nm.  $N_2^+$  molecular ions were produced by [2+1]-photon resonance enhanced photoionization from neutral nitrogen leaked into the vacuum chamber at a pressure of  $\approx 1 \times 10^{-8}$  mbar using a focused ns laser beam at 202 nm and sympathetically cooled into the center of the  $Ca^+$  crystal [14, 15]. After the ionisation, the  $N_2$  background pressure was maintained at that level for 30 seconds to equilibrate the rotational levels population by collisions and quench vibrational level populations to the ground state [32]. As demonstrated in Ref. [33], the sympathetically cooled  $N_2^+$  ions were converted into  $N_2H^+$  by leaking hydrogen gas into the trap chamber for 30 s at a pressure of  $\approx 1 \times 10^{-8}$  mbar.

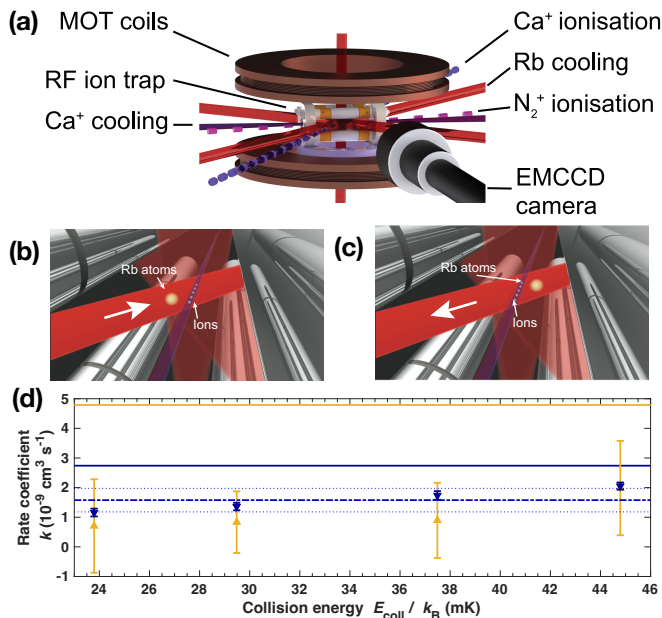


FIG. 1. (a) Schematic of the experiment consisting of a magneto-optical trap (MOT) for Rb atoms superimposed onto a radiofrequency (RF) linear-quadrupole ion trap. Laser beams are labeled by their functions. (b) and (c) schematic for shuttling the cloud of ultracold Rb atoms in between two extremal positions through a Coulomb crystal of ions. (d) Charge-transfer rate coefficients as a function of the  $N_2H^+$ -Rb collision energy for the  $(5s) ^2S_{1/2}$  ground state (blue  $\blacktriangledown$  symbols) and  $(5p) ^2P_{3/2}$  excited state (orange  $\blacktriangle$  symbols) of Rb. Blue (orange) solid line: Langevin rate constant in the Rb ground (excited) state. Dash-dotted and dashed lines: average experimental rate constant and its uncertainty limits. Error bars indicate the standard deviation of 5 measurements.

The MOT was continuously loaded from background Rb vapour replenished by an alkali-metal dispenser. Clouds of ultracold Rb atoms were generated in a position off-center from the ion trap (Fig. 1 (b)). The Rb atoms were then accelerated using radiation-pressure forces to pass through the Coulomb crystal at well-

defined velocities, recaptured after transit and sent back by applying radiation pressure in the opposite direction (Fig. 1 (c)). Repetition of the sequence for varying magnitudes of radiation pressure enabled the study of ion-atom collisions at variable, well-defined collision velocities [30]. Depending on whether the Rb cooling laser beams were switched off or on during transit, a part of the charge-transfer collisions between Rb and  $N_2H^+$  occurred in the  $(5p) ^2P_{3/2}$  excited state of Rb in addition to the  $(5s) ^2S_{1/2}$  ground state. The excitation fraction was determined from comparisons of the Rb fluorescence yields with an 8-level optical Bloch equation modelling as in Ref. [18]. Following Ref. [15], rate constants for charge-exchange reactions between  $N_2H^+$  and Rb were determined under pseudo-first-order-kinetics conditions for Rb by monitoring the depletion of the reactant ions from the crystal as a function of the time of exposure to the shuttling Rb atom cloud. The Rb density was extracted from a reference measurement of the  $O_2^+ + Rb$  reaction for which the rate coefficient conforms with the Langevin limit [15].

Fig. 1 (d) shows the charge-exchange rate coefficients, with Rb in either the  $(5s) ^2S_{1/2}$  ground state or the  $(5p) ^2P_{3/2}$  excited state, as functions of the collision energy in the interval  $E_{coll}/k_B \approx 23 - 45$  mK. Within the uncertainty limits, the rate coefficients are identical for both states across the studied energy interval, in contrast to  $N_2^+ + Rb$ , in which a marked difference between the two channels was found [15]. The larger uncertainty of the data for the excited state is due to the error in the determination of the excited-state population [15]. The rate constant for reactions with Rb in the ground state seems to exhibit a slight positive energy dependence across the energy range studied. Neglecting this effect, the average value is about a factor of 2 smaller than the corresponding Langevin rate coefficient, implying that the reaction rate is close to, but not equal to, the capture limit.

*Theory.* The reactants kinetic energy being nearly zero at temperatures of the order of few mK, endoenergetic reactions are impossible. It is shown in Fig. S-1 of the Supplemental Material (SM, [34]) that the only energetically accessible product channels are – aside from elastic or inelastic scattering – (a)  $N_2 + HRb^+$ , (b)  $N_2Rb^+ + H$  and (c)  $N_2 + H + Rb^+$ . Any of those channels can be reached in their electronic ground states only. Note that all those products involve an electron transfer from the rubidium atom to the hydrogen atom (even in the case of  $HRb^+$  the electron is essentially carried by H, as it is more electronegative than Rb). The neutral radical  $N_2H$  is unstable and readily dissociates to give  $N_2 + H$ , as already shown in previous works [35–39] (the metastable bent geometry [40] is neglected here). The  $N_2Rb$  radical is also unstable and can anyway not be observed as the channel  $N_2 + Rb + H^+$  is energetically inaccessible.

Fig. 2 shows the computed potential energy curves (PECs) of the linear  $N_2H$  and  $N_2H^+$  as functions of the

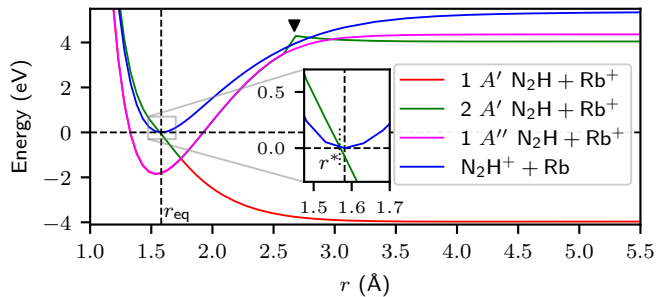


FIG. 2. Potential energy curves of linear  $\text{N}_2\text{H}$  and  $\text{N}_2\text{H}^+$  at infinite separation from  $\text{Rb}^+$  and  $\text{Rb}$ , respectively, as functions of the distance  $r$  between the center-of-mass of  $\text{N}_2$  and  $\text{H}$ . The  $\text{N}\equiv\text{N}$  bond distance is fixed at  $1.0945 \text{ \AA}$  and the dashed vertical line denotes the equilibrium value of  $r$  at  $r_{\text{eq}} = 1.5814 \text{ \AA}$  in  $\text{N}_2\text{H}^+$  [28]. Energies are relative to the threshold which corresponds to the minimum of the  $\text{N}_2\text{H}^+ + \text{Rb}$  potential (solid blue curve).  $\blacktriangledown$ : see computational methods in the SM [34].

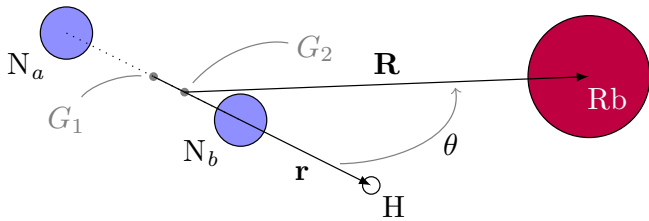


FIG. 3. Definition of the coordinates describing the arrangement of the nuclei in the  $[\text{N}_2\text{H}-\text{Rb}]^+$  system. The Jacobi vectors  $\mathbf{r}$  and  $\mathbf{R}$  are such that  $\mathbf{r}$  points from the center-of-mass of  $\text{N}_2$  ( $G_1$ ) to  $\text{H}$  and  $\mathbf{R}$  points from the center-of-mass of  $\text{N}_2\text{H}$  ( $G_2$ ) to  $\text{Rb}$ . The  $\text{N}\equiv\text{N}$  bond length is kept fixed and  $\text{H}$  stays along the  $\text{N}-\text{N}$  axis, as in Fig. 2. Within these constraints, the geometry of the system is fully determined by the distances  $r = |\mathbf{r}|$ ,  $R = |\mathbf{R}|$ , and the angle  $\theta$  between the two vectors.

distance  $r$  between  $\text{H}$  and the center of mass of  $\text{N}_2$  at fixed  $\text{N}\equiv\text{N}$  distance (methods are discussed in the SM [34]). These are corrected for the ionization energy of  $\text{Rb}$  so that they mimic the curves of  $\text{N}_2\text{H} + \text{Rb}^+$  and  $\text{N}_2\text{H}^+ + \text{Rb}$ , respectively, at infinite atom-cation separation. The  $\text{N}_2\text{H}^+ (+\text{Rb})$  potential is that of a bound species. The potential energy landscape of  $\text{N}_2\text{H} (+\text{Rb}^+)$  is more complex, featuring one steep dissociative state which crosses a pair of degenerate states, as already shown in Ref. [36]. The  $\text{N}_2\text{H} (+\text{Rb}^+)$  dissociative state plays the major role in the electron transfer process, as its PEC intersects that of  $\text{N}_2\text{H}^+ (+\text{Rb})$ . This intersection happens to be located at  $r^*$  slightly shorter than  $r_{\text{eq}} = 1.5814 \text{ \AA}$ , the  $\text{N}_2-\text{H}$  distance at the equilibrium geometry of  $\text{N}_2\text{H}^+$ , and drives the charge transfer  $\text{N}_2\text{H}^+ + \text{Rb} \rightarrow \text{N}_2\text{H} + \text{Rb}^+$  as the  $\text{Rb}$  atom approaches  $\text{N}_2\text{H}^+$ .

Thus, we computed the four lowest electronic eigenstates of the full tetra-atomic  $[\text{N}_2\text{H}-\text{Rb}]^+$  system identified in Fig. 2 as functions of the three coordinates  $r$ ,

$R$  and  $\theta$  defined in Fig. 3. Fig. 4 displays cuts of the corresponding PESs for  $\theta = 120^\circ$  (for other angles, see SM [34]). The system is initially in the diabatic  $\text{N}_2\text{H}^+ + \text{Rb}$  state at  $(r = r_{\text{eq}}, R \rightarrow \infty)$ . This corresponds to the solid blue curve at large  $R$  in Fig. 4 (a) and the bottom of the curve obtained by joining those of state  $2A'$  in green for  $r < r^*$  and  $3A'$  in blue for  $r > r^*$  in Fig. 4 (b). The intersection point at  $r^*$  shown in Fig. 2 is in fact an avoided crossing between the PECs in Fig. 4 (b) whose energy gap is exactly zero at  $R \rightarrow \infty$ .

For  $\text{N}_2\text{H}^+$  in its equilibrium geometry (solid curves in Fig. 4 (a)), the adiabatic PECs of states  $3A'$  and  $2A'$  feature an avoided crossing around  $R = 13.5 \text{ \AA}$  (see inset). There, the energy spacing between these states is still nearly zero. On the other hand, the attractive interaction between  $\text{N}_2\text{H}^+$  and  $\text{Rb}$  is such that the full system acquires enough kinetic energy to undergo a diabatic transition  $3A' \rightarrow 2A'$  with almost unit probability (dotted arrow in the inset of Fig. 4(a), see also Landau-Zener transition probabilities estimates in Table S-II in the SM [34]). However, for shorter distances  $R$ , the position of the avoided crossing varies in the vicinity of  $r_{\text{eq}}$  (see Fig. 4 (b)) and remains at energies below the entrance channel threshold. There, the energy gap between the two adiabatic states widens. Thus, for shorter  $R$ , diabatic transitions between the states  $3A'$  and  $2A'$  are less effective, giving chances to the system to stay adiabatically in the  $2A'$  state along the  $r$  coordinate (see Table S-II in the SM [34]). In other words, the system can leak from the parabolic part of the green PEC around  $r_{\text{eq}}$ , with  $\text{N}_2\text{H}^+ + \text{Rb}$  character, to the steep portion at  $r > r^*$  where the system gains  $\text{N}_2\text{H} + \text{Rb}^+$  character (solid arrow in Fig. 4 (b)). *This adiabatic passage is the manifestation of the electron transfer between  $\text{Rb}$  and  $\text{N}_2\text{H}^+$  which is promoted by a deformation of the molecule along the  $r$  coordinate.* The Landau-Zener model roughly predicts a 5% chance per pass to remain adiabatically in state  $2A'$ . However, the typical time spent by  $\text{Rb}$  in the vicinity of the cation ( $\approx 2.3 \text{ ps}$ ) is two orders of magnitude longer than the  $\text{N}_2-\text{H}^+$  stretching vibrational period ( $\approx 15 \text{ fs}$ ). Thus, the system has enough time to leak through the avoided crossing via this vibration (see SM [34] for timescales estimates). Once on the dissociative part of the  $2A'$  state PEC (green curves,  $r > r^*$ ), the system diabatically transits to its continuation on state  $1A'$  (see dotted arrow in Fig. 4 (b)), i.e.  $\text{H}$  readily dissociates from  $\text{N}_2$  as a result of the electron transfer from  $\text{Rb}$  to  $\text{N}_2\text{H}^+$ .

The discrepancy between the experimentally measured reaction rates and those predicted by the Langevin capture model is attributed to specific features of the PESs which are dependent on the angle of attack  $\theta$ . Fig. 5 shows two-dimensional contour plots in  $r$  and  $R$  of the PESs of states  $2A'$  and  $3A'$  cut at  $\theta = 0.01^\circ$  and  $\theta = 120^\circ$  (for other angles, see SM [34]). For each angle, the seam of avoided crossings from asymptotic separation

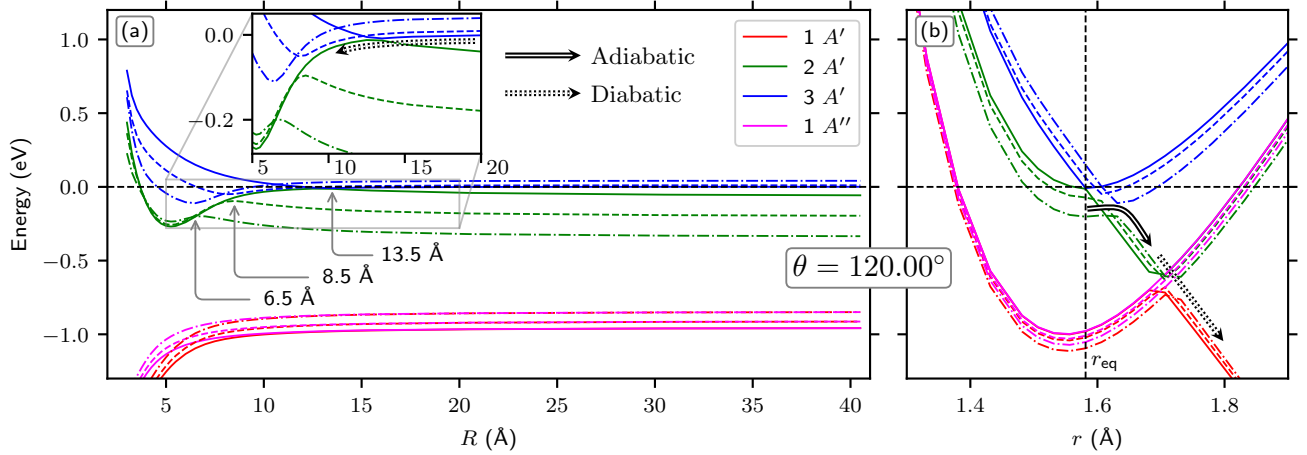


FIG. 4. Adiabatic potential energy surfaces cuts of the  $\text{N}_2\text{H}^+ + \text{Rb}$  system as functions of (a) the atom-cation distance  $R$  and (b) the  $\text{N}_2\text{--H}$  distance  $r$ , for  $\theta = 120^\circ$ . Note that, in panel (b), the state labeling/coloring is reversed compared to Fig. 2 for  $r$  shorter than  $r^*$  since here the electronic eigenstates are ordered by increasing energy (within a given irreducible representation). In (a) solid lines (—) correspond to cuts at  $r = r_{\text{eq}} = 1.5814 \text{ \AA}$ , dashed lines (---) at  $r = r_{\text{eq}} + 0.025 \text{ \AA}$  and dash-dotted lines (-.-) at  $r = r_{\text{eq}} + 0.050 \text{ \AA}$ . The indicated values of  $R$  locate the positions of the avoided crossings along those cuts. In (b), solid lines (—) correspond to cuts at  $R = 13.5 \text{ \AA}$ , dashed lines (---) at  $R = 8.5 \text{ \AA}$  and dash-dotted lines (-.-) at  $R = 6.5 \text{ \AA}$ . The dashed horizontal black lines denote the entrance channel energy. Double arrows indicate transitions described in the text.

towards finite distance  $R$  is traced by a minimum energy difference path (MEDP). As Fig. 5 shows, the PESs display a strong anisotropy at short range. Starting from the asymptote  $(r, R) \rightarrow (r_{\text{eq}}, +\infty)$  on state  $3A'$ , when the collision takes place on the H-side of  $\text{N}_2\text{H}^+$  ( $\theta \approx 0^\circ$ , Fig. 5 (a)), the region of coordinate space accessible by the system energy-wise is limited to distances  $R$  no shorter than approximately  $9 \text{ \AA}$ . In this region, the PES of state  $3A'$  is very shallow (the minimum is about  $0.034 \text{ eV}$  below the threshold) and the MEDP never crosses its boundary. The PES of state  $2A'$  underneath steeply decreases in energy both with increasing  $R$  and  $r$ , eventually becoming – in a diabatic sense – state  $1A'$  (see Fig. 4 (b)). The limited extent of the energy-allowed region and the increase of the energy gap between the states  $2A'$  and  $3A'$  therein forbids any non-adiabatic transition, hence no reaction takes place.

Conversely, when the collision occurs at  $\theta = 120^\circ$ , i.e. Rb approaches  $\text{N}_2\text{H}^+$  non-collinearly from the  $\text{N}_2$ -side (Fig. 5 (b)), the energy-allowed region of the PES of state  $3A'$  reaches points with  $R$  as close as  $4.2 \text{ \AA}$ . The lowest points in energy in this PES cut ( $\approx 0.13 \text{ eV}$  below the threshold) are close to the MEDP which, in this case, clearly enters inside that region. There, the energy gap between the PESs of states  $3A'$  and  $2A'$  is much smaller than in the  $\theta = 0^\circ$  case (see also Fig. S-6 in SM [34]). Hence, the latter state is more likely reached by non-adiabatic transition and the reaction occurs as discussed earlier in connection with Fig. 4. The case  $\theta = 60^\circ$  (see Fig. S-4 in the SM [34]), where the MEDP is nearly tangent to the energy-allowed region boundary, is close to the limit between the two behaviors described above.

*Conclusion.* Unaware of the structure of the cation, the Langevin capture model considers only the isotropic long-range ion-atom interaction, which is satisfactory when no other hindrance to the charge exchange arises at short range. However, our inspection of the distinctive interaction between  $\text{N}_2\text{H}^+$  and Rb at short range, necessarily anisotropic, reveals that an efficient charge transfer in the cold regime cannot occur from all angles of attack because of the above-mentioned obstacles encountered for  $\theta < 60^\circ$ , i.e. for about one third of the configuration space spanned by  $\theta$ . Although the orientation of the cation is not locked during the collision as Fig. 5 may suggest (see SM [34]) these obstacles are nonetheless a limitation to a successful reaction and are qualitatively reflected in the experimental reaction rates which are roughly half of the Langevin prediction.

The anisotropy of the potentials also precludes the formation of the  $\text{HRb}^+$  product. From a steric point of view, the proton capture by Rb should be eased by an attack around  $\theta = 0^\circ$ , but no effective electronic transition allows the formation of the  $\text{H} \cdots \text{Rb}^+$  bond leaving no other option than scattering of Rb away from  $\text{N}_2\text{H}^+$ . Conversely, the attack of Rb from the  $\text{N}_2$ -side does allow the electron transfer, leading to the formation of the ephemeral  $\text{N}_2\text{H}$  radical. Due to the steep dissociative character of the PES of state  $2A'$  (and its diabatic continuation in state  $1A'$ ), the radical readily dissociates into  $\text{N}_2 + \text{H}$ .

*Summary.* We have studied the charge exchange of a polyatomic ion with Rb in an ion-atom hybrid trap. At the present mK collision energies, the system was found to only sample parts of the available configuration space



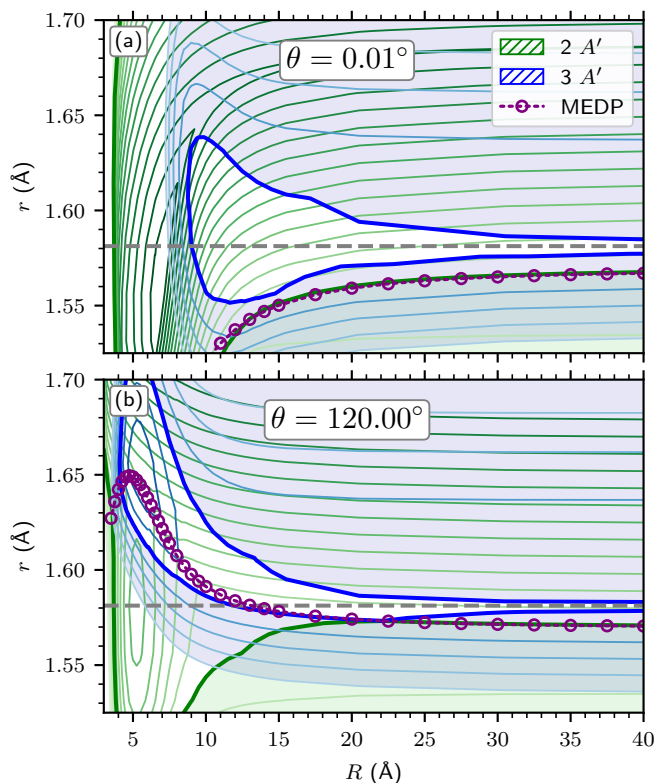


FIG. 5. Contour plots of the PESs of states  $2A'$  and  $3A'$  as functions of  $r$  and  $R$  for (a)  $\theta = 0.01^\circ$  and (b)  $\theta = 120.00^\circ$ . The thick green and blue contour lines correspond to the threshold energy  $E = 0$  in those states, respectively. Other isoenergetic contours are traced every 0.05 eV. Shaded areas indicate energy-forbidden regions of configuration space on the corresponding PES. The dashed grey line indicates the entrance asymptotic channel ( $r = r_{eq}$ ,  $R \rightarrow \infty$ ).

of the reaction so that charge transfer becomes highly geometry dependent, is promoted by a deformation of the molecule and thus becomes slower than the Langevin limit. The present study underlines the role of stereodynamics and polyatomic effects in cold collisions of molecular ion-neutral systems.

**Acknowledgments.** AV thanks T. Véry and R. Lacroix for extensive support in the usage of the Jean-Zay CNRS-IDRIS supercomputer. AV thanks Amrendra Pandey (Laboratoire Aimé Cotton) for fruitful discussions at the early stage of the computational work and the MOLPRO development team for technical assistance. LW thanks J. Brandão (U. Algarve, PT) for many early discussions. This work is supported by Investissements d'Avenir, LabEx PALM (ANR-10-LABX-0039-PALM), Université Paris-Saclay, the Swiss National Science Foundation (grants nr. 200020.175533 and TMAG-2.209193) and the University of Basel. Computation on the Jean-Zay CNRS-IDRIS supercomputer was made possible thanks to contract A0120810769.

AV and AD contributed equally to this work.

\* Corresponding author: alexandre.voute@universite-paris-saclay.fr

† Corresponding author: stefan.willitsch@unibas.ch

- [1] Michał Tomza, Krzysztof Jachymski, Rene Gerritsma, Antonio Negretti, Tommaso Calarco, Zbigniew Idziaszek, and Paul S Julienne, “Cold hybrid ion-atom systems,” *Rev. Mod. Phys.* **91**, 035001 (2019).
- [2] C. Zipkes, S. Palzer, C. Sias, and M. Köhl, “A trapped single ion inside a Bose–Einstein condensate,” *Nature* **464**, 388 (2010).
- [3] K. Ravi, S. Lee, A. Sharma, G. Werth, and S. A. Rangwala, “Sympathetic and swap cooling of trapped ions by cold atoms in a MOT,” *Nat. Commun.* **3**, 1126 (2012).
- [4] A. Mahdian, A. Krüchow, and J. H. Denschlag, “Direct observation of swap cooling in atom–ion collisions,” *New J. Phys.* **23**, 065008 (2021).
- [5] W. G. Rellergert, S. T. Sullivan, S. J. Schowalter, S. Kotochigova, K. Chen, and E. R. Hudson, “Evidence for sympathetic vibrational cooling of translationally cold molecules,” *Nature* **495**, 490 (2013).
- [6] F. H. J. Hall, M. Aymar, N. Bouloufa-Maafa, O. Dulieu, and S. Willitsch, “Light-Assisted Ion-Neutral Reactive Processes in the Cold Regime: Radiative Molecule Formation versus Charge Exchange,” *Phys. Rev. Lett.* **107**, 243202 (2011).
- [7] M. Mills, P. Puri, M. Li, S. J. Schowalter, A. Dunning, C. Schneider, S. Kotochigova, and E. R. Hudson, “Engineering Excited-State Interactions at Ultracold Temperatures,” *Phys. Rev. Lett.* **122**, 233401 (2019).
- [8] A. Krüchow, A. Mohammadi, A. Härter, J. H. Denschlag, J. Pérez-Ríos, and C. H. Greene, “Energy Scaling of Cold Atom-Atom-Ion Three-Body Recombination,” *Phys. Rev. Lett.* **116**, 193201 (2016).
- [9] Ziv Meir, Tomas Sikorsky, Ruti Ben-Shlomi, Nitzan Akerman, Yehonatan Dallal, and Roee Ozeri, “Dynamics of a Ground-State Cooled Ion Colliding with Ultracold Atoms,” *Phys. Rev. Lett.* **117**, 243401 (2016).
- [10] T. Feldker, H. FÜRST, H. Hirzler, N. V. Ewald, M. Mazzanti, D. Wiater, M. Tomza, and R. Gerritsma, “Buffer gas cooling of a trapped ion to the quantum regime,” *Nat. Phys.* **16**, 413 (2020).
- [11] P. Weckesser, F. Thielemann, D. Wiater, A. Wojciechowska, L. Karpa, K. Jachymski, M. Tomza, T. Walker, and T. Schaetz, “Observation of Feshbach resonances between a single ion and ultracold atoms,” *Nature* **600** (2021).
- [12] O. Katz, M. Pinkas, N. Akerman, and R. Ozeri, “Quantum logic detection of collisions between single atom–ion pairs,” *Nat. Phys.* **18**, 533 (2022).
- [13] S. Schmid, A. Härter, and J. H. Denschlag, “Dynamics of a cold trapped ion inside a Bose–Einstein condensate,” *Phys. Rev. Lett.* **105**, 133202 (2010).
- [14] F. H. J. Hall and S. Willitsch, “Millikelvin reactive collisions between sympathetically cooled molecular ions and laser-cooled atoms in an ion-atom hybrid trap,” *Phys. Rev. Lett.* **109**, 233202 (2012).
- [15] A. D. Dörfler, P. Eberle, D. Koner, M. Tomza, M. Meuwly, and S. Willitsch, “Long-range versus short-range effects in cold molecular ion-neutral collisions,” *Nat. Commun.* **10**, 5429 (2019).
- [16] M. Tacconi, F. A. Gianturco, and A. K. Belyaev, “Com-

- puting charge-exchange cross sections for  $\text{Ca}^+$  collisions with Rb at low and ultralow energies,” *Phys. Chem. Chem. Phys.* **13**, 19156 (2011).
- [17] X. Xing, H. da Silva, R. Vexiau, N. Bouloufa-Maafa, S. Willitsch, and O. Dulieu, “Ion-loss events in a hybrid trap of cold  $\text{Rb}-\text{Ca}^+$ : Photodissociation, blackbody radiation, and nonradiative charge exchange,” *Phys. Rev. A* **106**, 062809 (2022).
- [18] F. H. J. Hall, P. Eberle, G. Hegi, M. Raoult, M. Aymar, O. Dulieu, and S. Willitsch, “Ion-neutral chemistry at ultralow energies: dynamics of reactive collisions between laser-cooled  $\text{Ca}^+$  ions and Rb atoms in an ion-atom hybrid trap,” *Mol. Phys.* **111**, 2020 (2013).
- [19] L. Ratschbacher, C. Zipkes, C. Sias, and M. Köhl, “Controlling Chemical Reactions of a Single Particle,” *Nat. Phys.* **8**, 649 (2012).
- [20] Prateek Puri, Michael Mills, Christian Schneider, Ionel Simbotin, John A. Montgomery, Robin Côté, Arthur G. Suits, and Eric R. Hudson, “Synthesis of mixed hypermetallic oxide  $\text{BaOCa}^+$  from laser-cooled reagents in an atom-ion hybrid trap,” *Science* **357**, 1370 (2017).
- [21] H. Hirzler, R. S. Lous, E. Trimby, J. Pérez-Rios, A. Safavi-Naini, and R. Gerritsma, “Observation of Chemical Reactions between a Trapped Ion and Ultracold Feshbach Dimers,” *Phys. Rev. Lett.* **128**, 103401 (2022).
- [22] P. Thaddeus and B. E. Turner, “Confirmation of interstellar  $\text{N}_2\text{H}^+$ ,” *Astrophys. J.* **201**, L25 (1975).
- [23] Richard J. Saykally, Thomas A. Dixon, Thomas G. Anderson, Peter G. Szanto, and R. Claude Woods, “Laboratory microwave spectrum and rest frequencies of the  $\text{N}_2\text{H}^+$  ion,” *Astrophys. J.* **205**, L101 (1976).
- [24] Christopher S. Gudeman, Marianne H. Begemann, Jürgen Pfaff, and Richard J. Saykally, “Velocity-modulated infrared laser spectroscopy of molecular ions: The  $\nu_1$  band of  $\text{HNN}^+$ ,” *J. Chem. Phys.* **78**, 5837–5838 (1983).
- [25] S. C. Foster and A. R. W. McKellar, “The  $\nu_3$  fundamental bands of  $\text{HN}_2^+$ ,  $\text{DN}_2^+$ , and  $\text{DCO}^+$ ,” *J. Chem. Phys.* **81**, 3424–3428 (1984).
- [26] Trevor J. Sears, “Observation of the  $\nu_2$  (bending) fundamental of the  $\text{HN}_2^+$  ion at 146 micrometers,” *J. Opt. Soc. Am. B* **2**, 786 (1985).
- [27] S. Forsén and B. Roos, “MO SCF studies of the protonation of carbon monoxide and the nitrogen molecule using gaussian basis sets,” *Chem. Phys. Lett.* **6**, 128–132 (1970).
- [28] V. Brites and M. Hochlaf, “Titan’s Ionic Species: Theoretical Treatment of  $\text{N}_2\text{H}^+$  and Related Ions,” *J. Phys. Chem. A* **113**, 11107–11111 (2009).
- [29] X. Huang, E. F. Valeev, and T. J. Lee, “Comparison of one-particle basis set extrapolation to explicitly correlated methods for the calculation of accurate quartic force fields, vibrational frequencies, and spectroscopic constants: Application to  $\text{H}_2\text{O}$ ,  $\text{N}_2\text{H}^+$ ,  $\text{NO}_2^+$ , and  $\text{C}_2\text{H}_2$ ,” *J. Chem. Phys.* **133**, 244108 (2010).
- [30] Pascal Eberle, Alexander D. Dörfler, Claudio von Planta, Krishnamurthy Ravi, and Stefan Willitsch, “A Dynamic Ion-Atom Hybrid Trap for High-Resolution Cold-Collision Studies,” *ChemPhysChem* **17**, 3769–3775 (2016).
- [31] S. Willitsch, “Coulomb-crystallised molecular ions in traps: methods, applications, prospects,” *Int. Rev. Phys. Chem.* **31**, 175 (2012).
- [32] X. Tong, T. Nagy, J. Yosa Reyes, M. Germann, M. Meuwly, and S. Willitsch, “State-selected ion-molecule reactions with Coulomb-crystallized molecular ions in traps,” *Chem. Phys. Lett.* **547**, 1–8 (2012).
- [33] Ardita Kilaj, Hong Gao, Daniel Rösch, Uxia Rivero, Jochen Küpper, and Stefan Willitsch, “Observation of different reactivities of para and ortho-water towards trapped diazenylium ions,” *Nat. Commun.* **9**, 2096 (2018).
- [34] See Supplemental Material for the computation of asymptotic energies with methods described in [41–45] using MOLPRO [46–48]; excited state energies at the asymptotes estimated using data from [49–54]; computation of the  $\text{N}_2\text{H}^+$  and  $\text{N}_2\text{H}$  potential energy curves with methods described in [55–61]; diabatic transition probabilities calculated using data from [25]; relevant timescales estimated using data from [25, 62].
- [35] Susan F. Selgren, Patrick W. McLoughlin, and Gregory I. Gellene, “Observation of dissociative and radiative states of  $\text{N}_2\text{H}$  by neutralized ion beam techniques,” *J. Chem. Phys.* **90**, 1624–1629 (1989).
- [36] Vinícius C. Mota and António J. C. Varandas, “ $\text{HN}_2$  ( $^2A'$ ) Electronic Manifold. II. Ab Initio Based Double-Sheeted DMBE Potential Energy Surface via a Global Diabatization Angle,” *J. Phys. Chem. A* **112**, 3768–3786 (2008).
- [37] D. Talbi, “A quantum chemical study of the  $\text{N}_2\text{H}^+ + e^- \rightarrow \text{N}_2 + \text{H}$  reaction, I: The linear dissociation path,” *Chem. Phys.* **332**, 298–303 (2007).
- [38] D.O. Kashinski, D. Talbi, and A.P. Hickman, “Ab initio calculations of autoionizing states using block diagonalization: Collinear diabatic states for dissociative recombination of electrons with  $\text{N}_2\text{H}^+$ ,” *Chem. Phys. Lett.* **529**, 10–15 (2012).
- [39] D.O. Kashinski, D. Talbi, and A.P. Hickman, “Using block diagonalization to determine dissociating autoionizing states: Application to  $\text{N}_2\text{H}$ , and the outlook for  $\text{SH}$ ,” *EPJ Web Conf.* **84**, 03003 (2015).
- [40] Uğur Bozkaya, Justin M. Turney, Yukio Yamaguchi, and Henry F. Schaefer, “The barrier height, unimolecular rate constant, and lifetime for the dissociation of  $\text{HN}_2$ ,” *J. Chem. Phys.* **132**, 064308 (2010).
- [41] Krishnan Raghavachari, Gary W. Trucks, John A. Pople, and Martin Head-Gordon, “A fifth-order perturbation comparison of electron correlation theories,” *Chem. Phys. Lett.* **157**, 479–483 (1989).
- [42] Claudia Hampel, Kirk A. Peterson, and Hans-Joachim Werner, “A comparison of the efficiency and accuracy of the quadratic configuration interaction (QCISD), coupled cluster (CCSD), and Brueckner coupled cluster (BCCD) methods,” *Chem. Phys. Lett.* **190**, 1–12 (1992).
- [43] Thom H. Dunning, “Gaussian basis sets for use in correlated molecular calculations. I. The atoms boron through neon and hydrogen,” *J. Chem. Phys.* **90**, 1007–1023 (1989).
- [44] Rick A. Kendall, Thom H. Dunning, and Robert J. Harrison, “Electron affinities of the first-row atoms revisited. Systematic basis sets and wave functions,” *J. Chem. Phys.* **96**, 6796–6806 (1992).
- [45] J. G. Hill and K. A. Peterson, “Gaussian basis sets for use in correlated molecular calculations. XI. Pseudopotential-based and all-electron relativistic basis sets for alkali metal (K–Fr) and alkaline earth (Ca–Ra) elements,” *J. Chem. Phys.* **147**, 244106 (2017).

- [46] H.-J. Werner, P. J. Knowles, G. Knizia, F. R. Manby, M. Schütz, P. Celani, W. Györffy, D. Kats, T. Korona, R. Lindh, A. Mitrushenkov, G. Rauhut, K. R. Shamasundar, T. B. Adler, R. D. Amos, S. J. Bennie, A. Bernhardtson, A. Berning, D. L. Cooper, M. J. O. Deegan, A. J. Dobbyn, F. Eckert, E. Goll, C. Hampel, A. Hesselmann, G. Hetzer, T. Hrenar, G. Jansen, C. Köppl, S. J. R. Lee, Y. Liu, A. W. Lloyd, Q. Ma, R. A. Mata, A. J. May, S. J. McNicholas, W. Meyer, T. F. Miller III, M. E. Mura, A. Nicklass, D. P. O'Neill, P. Palmieri, D. Peng, K. Pflüger, R. Pitzer, M. Reiher, T. Shiozaki, H. Stoll, A. J. Stone, R. Tarroni, T. Thorsteinsson, M. Wang, and M. Welborn, "MOLPRO, version 2022.1, a package of ab initio programs,".
- [47] H.-J. Werner, P. J. Knowles, G. Knizia, F. R. Manby, and M. Schütz, "Molpro: a general-purpose quantum chemistry program package," *WIREs Comput. Mol. Sci.* **2**, 242–253 (2012).
- [48] Hans-Joachim Werner, Peter J. Knowles, Frederick R. Manby, Joshua A. Black, Klaus Doll, Andreas Heßelmann, Daniel Kats, Andreas Köhn, Tatiana Korona, David A. Kreplin, Qianli Ma, Thomas F. Miller, Alexander Mitrushchenkov, Kirk A. Peterson, Iakov Polyak, Guntram Rauhut, and Marat Sibaev, "The Molpro quantum chemistry package," *J. Chem. Phys.* **152**, 144107 (2020).
- [49] Ingmar Johansson, "Spectra of the alkali metals in the lead-sulphide region," *Ark. Fys.* **20**, 135 (1961).
- [50] J. E. Sansonetti, "Wavelengths, Transition Probabilities, and Energy Levels for the Spectra of Rubidium (Rb I through Rb XXXVII)," *J. Phys. Chem. Ref. Data* **35**, 301–421 (2006).
- [51] R. E. Miller, "The absolute energy of the  $A^3\Sigma_u^+$  state of nitrogen," *J. Mol. Spec.* **19**, 185–187 (1966).
- [52] T. Trickl, E. F. Cromwell, Y. T. Lee, and A. H. Kung, "State-selective ionization of nitrogen in the  $X^2\Sigma_g^+ v_+ = 0$  and  $v_+ = 1$  states by two-color (1+1) photon excitation near threshold," *J. Chem. Phys.* **91**, 6006–6012 (1989).
- [53] Lingling Yan, Yizhi Qu, Chunhua Liu, Jianguo Wang, and Robert J. Buenker, "Ab initio many-electron study for the low-lying states of the alkali hydride cations in the adiabatic representation," *J. Chem. Phys.* **136**, 124304 (2012).
- [54] Mireille Aymar, Johannes Deiglmayr, and Olivier Dulieu, "Systematic trends in electronic properties of alkali hydrides," *Can. J. Phys.* **87**, 543–556 (2009).
- [55] H.-J. Werner and Peter J. Knowles, "An Efficient Internally Contracted Multiconfiguration Reference CI Method," *J. Chem. Phys.* **89**, 5803–5814 (1988).
- [56] Peter J. Knowles and H.-J. Werner, "An Efficient Method for the Evaluation of Coupling Coefficients in Configuration Interaction Calculations," *Chem. Phys. Lett.* **145**, 514–522 (1988).
- [57] Peter J. Knowles and Hans-Joachim Werner, "Internally contracted multiconfiguration-reference configuration interaction calculations for excited states," *Theor. Chem. Acc.* **84**, 95–103 (1992).
- [58] Michael P. Deskevich, David J. Nesbitt, and Hans-Joachim Werner, "Dynamically weighted multiconfiguration self-consistent field: Multistate calculations for  $F + H_2O \rightarrow HF + OH$  reaction paths," *J. Chem. Phys.* **120**, 7281–7289 (2004).
- [59] Hans-Joachim Werner and Peter J. Knowles, "A second order multiconfiguration SCF procedure with optimum convergence," *J. Chem. Phys.* **82**, 5053–5063 (1985).
- [60] Peter J. Knowles and H.-J. Werner, "An Efficient Second Order MCSCF Method for Long Configuration Expansions," *Chem. Phys. Lett.* **115**, 259–267 (1985).
- [61] David A. Kreplin, Peter J. Knowles, and Hans-Joachim Werner, "Second-order MCSCF optimization revisited. I. Improved algorithms for fast and robust second-order CASSCF convergence," *J. Chem. Phys.* **150**, 194106 (2019).
- [62] T. Amano, T. Hirao, and J. Takano, "Submillimeter-wave spectroscopy of  $HN_2^+$  and  $DN_2^+$  in the excited vibrational states," *J. Mol. Spec.* **234**, 170–175 (2005).